Journal of Theoretical Biology 508 (2021) 110452

Contents lists available at ScienceDirect

Journal of Theoretical Biology

journal homepage: www.elsevier.com/locate/yjtbi

Inflected wings in flight: Uniform flow of stresses makes strong and light wings for stable flight

Pezhman Mardanpour [a,*], Ehsan Izadpanahi [a], Shanae Powell [a], Siavash Rastkar [a], Adrian Bejan [b]

[a] Florida International University, Miami, Florida 33174, USA
[b] Duke University, Durham, North Carolina 27708-0300, USA

ARTICLE INFO

Article history:
Received 25 March 2020
Revised 29 July 2020
Accepted 9 August 2020
Available online 20 August 2020

Keywords:
Design
Inflected wing
Flow of stresses
Flutter

ABSTRACT

Flying animals morph and flex their wings during their flight. Their wings morph with the turbulent flow created around them. The wings of modern airplanes do not have this ability. In this study we show that the ability to flex the wings leads to greater stability (higher flutter speed), and that this is due to the more uniform distribution of stresses in the flexing wing. This way the flexing wing becomes the lightest per unit of flapping force, or the strongest per unit of weight.

1. Introduction

The evolutionary design of flight in nature provides a very efficient mechanism for locomotion of more than a million insect species (Dudley, 2002), 1000 species of bats and almost 10,000 bird species (Chin and Lentink, 2016). The complex wing behavior makes these animals capable of performing sophisticated flight maneuvers such as flying sideways, taking off backward, making sharp turns, aiming at targets and hovering.

Following the evolution of birds and, in particular, the way their wings and feathers have evolved shows adaptations in their geometries for different needs and purposes. For instance, in order to suppress the aerodynamic noise, owls have evolved over 20 million years to perfect their wings geometry and properties and become the only vehicle known to the man capable of almost silent flight (Lilley, 1998; Jaworski and Peake, 2013; Agrawal and Sharma, 2016; Mandadzhiev et al., 2017; Jaworski and Peake, 2020). This efficient design of flying animals inspired the design of airplanes (Van Dam, 1987; Lentink et al., 2007), and the biology fields of animal design and the physics of living systems (Wainwright et al., 1976; Schmidt-Nielsen, 1984; Vogel, 1988; Weibel et al., 1998; Ahlborn, 2004; Bejan, 2016).

The evolution of the models of airplanes toward the configurations and scaling laws of flying animals illustrates convincingly the similarities between the two groups (Bejan and Marden, 2006, 2009). Yet, the airplane design continues to lag behind the animal design in one important respect: the animal wing is capable of flexing in all directions, all along its length and at any time during flight. The wing of the bird goes with the flow around it, and it morphs in flight. This is a common feature of birds of all sizes, as shown in Fig. 1 (Vogel, 1988; Bejan, 2020).

In this paper we show how the aeroelastic (fluid–structure interaction) design of the airplane wing returns the favor to the animal design by revealing the physics of the wing that flexes and goes with the flow. The physics is the tendency of the wing to morph with freedom such that the stresses are distributed as uniformly as possible through its body at any time. This tendency allows the wing to be the lightest per unit of flapping force, or the strongest per unit of weight. This tendency toward "svelteness" unites all bodies with locomotion (Bejan and Marden, 2006, 2009), as the power spent on movement is proportional to the body size.

The connection between natural body architecture and uniform distribution of stresses was proposed in the Journal of Theoretical Biology as a way to predict the architecture of trees (Bejan et al., 2008). Vegetation design belongs to a wider domain of evolutionary design underpinned by the same principle, for example animal locomotion (Bejan and Marden, 2006), corals and bacterial colonies (Miguel, 2006), ant mounds (Kasimova et al., 2014), human lungs (Reis et al., 2004), and tree networks (Miguel, 2016).

* Corresponding author at: Department of Mechanical and Materials Engineering, Florida International University, 10555 W Flagler St, Miami, FL 33174, USA.
E-mail address: Pezhman.Mardanpour@FIU.edu (P. Mardanpour).

https://doi.org/10.1016/j.jtbi.2020.110452
0022-5193/

Nomenclature

a	Deformed beam aerodynamic frame of reference
b	Undeformed beam cross-sectional frame of reference
B	Deformed beam cross-sectional frame of reference
$\mathbf{b}_i$	Unit vectors in undeformed beam cross-sectional frame of reference ($i = 1, 2, 3$)
$\mathbf{B}_i$	Unit vectors of deformed beam cross-sectional frame of reference ($i = 1, 2, 3$)
c	Chord
C^{bi}	Transformation matrix from the inertial frame i to undeformed beam frame b
C^{Bi}	Transformation matrix from the inertial frame i to deformed beam frame B
C^{ib}	Transformation matrix from the undeformed beam frame b to inertial frame i
C^{iB}	Transformation matrix from the deformed beam frame B to inertial frame i
c_{d_0}, c_{l_0}	Aerodynamic drag and lift coefficients at zero angle of attack
$c_{m\beta}$	Pitch moment coefficient w.r.t. flap deflection (β)
$c_{l\alpha}$	Lift coefficient w.r.t. angle of attack (α)
$c_{l\beta}$	Lift coefficient w.r.t. flap deflection (β)
e_1	Column matrix
e	Offset of aerodynamic center from the origin of frame of reference along $\mathbf{b}_2$
f	Column matrix of distributed, applied force measured in $\mathbf{B}_i$ basis
F	Column matrix of internal force measured in $\mathbf{B}_i$ basis
$\mathbf{g}$	Gravitational vector in $\mathbf{B}_i$ basis
H	Column matrix of cross-sectional angular momentum measured in $\mathbf{B}_i$ basis
i	Inertial frame of reference
$\mathbf{i}_i$	Unit vectors for inertial frame of reference ($i = 1, 2, 3$)
I	Cross-sectional inertia matrix
k	Column matrix of undeformed beam initial curvature and twist measured in $\mathbf{b}_i$ basis
K	Column matrix of deformed beam curvature and twist measured in $\mathbf{B}_i$ basis
m	Column matrix of distributed, applied moment measured in $\mathbf{B}_i$ basis
M	Column matrix of internal moment measured in $\mathbf{B}_i$ basis
P	Column matrix of cross-sectional linear momentum measured in $\mathbf{B}_i$ basis
r	Column matrix of position vector measured in $\mathbf{b}_i$ basis
u	Column matrix of displacement vector measured in $\mathbf{b}_i$ basis
V	Column matrix of velocity measured in $\mathbf{B}_i$ basis
x_1	Axial coordinate of beam
α	Angle of attack
β	Trailing edge flap angle
γ	Column matrix of 1D generalized force strain measures
Δ	Identity matrix
κ	Column matrix of elastic twist and curvature measures
λ	Column matrix of induced flow states
μ	Mass per unit length
ξ	Column matrix of center of mass offset from the frame of reference origin
ρ	Air density
ψ	Column matrix of small incremental rotations
Ω	Column matrix of cross-sectional angular velocity
$(\,)'$	Partial derivative with respect to x_1
$\dot{(\,)}$	Partial derivative with respect to time
$\hat{(\,)}$	Nodal variable

2. Aeroelastic design

The progress toward "better" human flight (i.e., higher, farther, faster, and more affordable) has been a challenge. One barrier has been "flutter", or dynamic aeroelastic instability. The state-of-the-art aeroelastic design and analysis methods are capable of describing aeroelastic instabilities, but they come short of illuminating the reasons behind the occurrence of such instabilities.

Wing inflection and curvature has the potential to postpone the speed at which these instabilities occur. There is a research literature on curvature in the chord-wise direction (Chiarelli et al., 2009, 2010, 2011; Sofla et al., 2010; Galantai et al., 2012; Nguyen et al., 2013), curvature along the wing (i.e., span-wise direction) (Sofla et al., 2010; Nguyen et al., 2013), and at the leading edge (Dora, 2018; Khan and Al-Faruk, 2018). The inflected wing in the present paper was inspired by work at NASA (Nguyen et al., 2013), where the primary purpose was to investigate the effect of curvature along the span (inflection and drooping) on lift and drag. The NASA work showed that curvature improves the aerodynamic characteristics of the aircraft, yet, there is no study in the literature that addressed the effect of wing inflection on aeroelastic stability. Here, we consider this question.

The concept of "flow of stresses" was introduced by Bejan and coworkers (Bejan and Lorente, 2008; Bejan et al., 2008; Lorente et al., 2010). They demonstrated the flow evolution analogy between the configuring of heat and fluid flow and the configuring of the flow of stresses, and showed that the avoidance of flow strangulation is the universal principle that accounts for both. By viewing solid structures as flow systems that configure and morph to accommodate the flow of stresses, they investigated solid structures in which stresses flow without strangulation. This led to the conclusion that such structures are the strongest and the lightest.

For example, in the analysis of a Y-shaped loaded structure that allows the flow of stresses so that the load is maximal when the volume is fixed, or the volume is minimal when the load is fixed, the best design under several failure mechanisms (buckling, pure compression, or pure tension) varied according to the failure mechanism. The flow of stresses is a vital part of the evolutionary design phenomenon oriented toward easier and safer flow access, in all flow systems with freedom to move and morph, animate and inanimate (Bejan, 2020).

3. Aeroelastic theory and simulation process

The chief objective of this work is to explain why wing inflection increases or decreases the flutter speed of a flying wing. To achieve this, we compare the flutter characteristics and the flow of stresses of a flying wing with inflection with a reference model that does not have wing inflection.

The sectional geometry of the fuselage and the wing is created using Gmsh mesh generator. The sectional properties of the wing are derived from Variational Asymptotic Beam Sectional Analysis (VABS) (Yu et al., 2002a; Yu and Hodges, 2005; Yu et al., 2012). The simulation software Nonlinear Aeroelastic Trim And Stability of HALE Aircraft (NATASHA) (where HALE stands for High Altitude Long Endurance) (Patil and Hodges, 2006; Chang et al., 2008) uses this information to assess the stability of the aircraft due to small

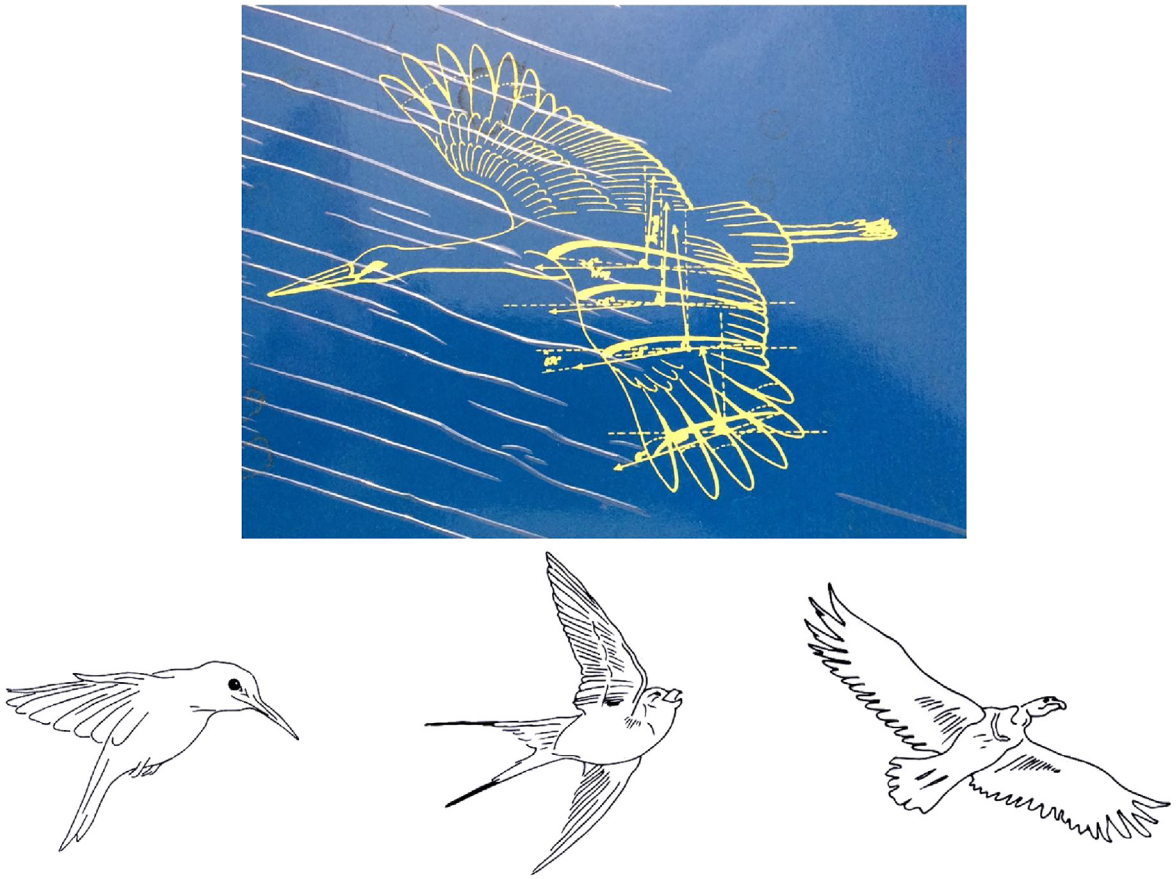

Fig. 1. Top: Avian aerodynamics (Vogel, 1988). Bottom: Inflected wings in bird flight (hummingbird, barn swallow, condor): in big birds the wings occupy a larger fraction of the body volume (Bejan, 2020).

perturbation about equilibrium configurations. For a specified subcritical speed (i.e., a speed below flutter speed for all inflected aircraft configurations), the computer program NATASHA finds the equilibrium configurations (called "trim" configurations) and assesses the stability of the aircraft, and the stress recovery module of the computer program VABS depicts the flow of stresses through the wings.

The fully intrinsic nonlinear composite beam theory (Hodges, 2003) is based on first-order partial differential equations of motion, the intrinsic kinematic partial differential equations, and the structural and the inertial constitutive equations. These equations are independent of displacement and rotation variables. The equations are geometrically exact, fully intrinsic, and they account for the dynamical behavior of a general, nonuniform, twisted, curved, anisotropic beams undergoing large deformation.

The equations of motion account for force, moment, angular velocity and velocity with nonlinearities of second order (Mardanpour et al., 2013, 2014, 2017a,b; Izadpanahi and Mardanpour, 2018; Mardanpour et al., 2018). The variables can be expressed with reference to the cross-sectional reference frames for the undeformed and deformed beam, $B(x_1,t)$ and $b(x_1)$, respectively, cf. Fig. 2. Here F_B and M_B are the column matrices of cross-sectional stress and moment resultant; V_B and Ω_B are the column matrices of cross-sectional frame velocity and angular velocity; P_B and H_B are the column matrices of cross-sectional linear and angular momentum measures; $\widetilde{K}_B$ is the column matrix of the curvature and twist of the deformed beam. The variables are in $\mathbf{B}_i$ basis. More details of this method can be found in Refs. Hodges (2003), Mardanpour et al. (2013, 2014, 2017a,b), Izadpanahi and Mardanpour (2018), Mardanpour et al. (2018) and the Nomenclature.

The structural and the inertial constitutive equations are:

$$F_B' + \widetilde{K}_B F_B + f_B = \dot{P}_B + \widetilde{\Omega}_B P_B M_B' + \widetilde{K}_B M_B + \left(\widetilde{e}_1 + \widetilde{\gamma}\right) F_B + m_B = \dot{H}_B + \widetilde{\Omega}_B H_B + \widetilde{V}_B P_B \tag{1}$$

$$\begin{Bmatrix} \gamma \\ \kappa \end{Bmatrix} = \begin{bmatrix} R & S \\ S^T & T \end{bmatrix} \begin{Bmatrix} F_B \\ M_B \end{Bmatrix} \tag{2}$$

$$\begin{Bmatrix} P_B \\ H_B \end{Bmatrix} = \begin{bmatrix} \mu\Delta & -\mu\widetilde{\xi} \\ \mu\widetilde{\xi} & I \end{bmatrix} \begin{Bmatrix} V_B \\ \Omega_B \end{Bmatrix} \tag{3}$$

where R, S, and T represent 3×3 partitions of the cross-sectional flexibility matrix; γ is the column matrix of 1D generalized force strain; κ is the column matrix of elastic twist and curvature; μ is the mass per unit length; Δ is the 3×3 identity matrix; I is the 3×3 cross-sectional inertia matrix; ξ is $\lfloor 0 \;\; \xi_2 \;\; \xi_3 \rfloor^T$ in which ξ_2 and ξ_3 represent the position coordinates of the cross-sectional mass center with respect to the reference line. Finally, strain–displacement and velocity-displacement equations are used to derive the intrinsic kinematic partial differential equations (Hodges, 2003).

$$V_B' + \widetilde{K}_B V_B + \left(\widetilde{e}_1 + \widetilde{\gamma}\right)\Omega_B = \dot{\gamma} \tag{4}$$

$$\Omega_B' + \widetilde{K}_B \Omega_B = \dot{\kappa} \tag{5}$$

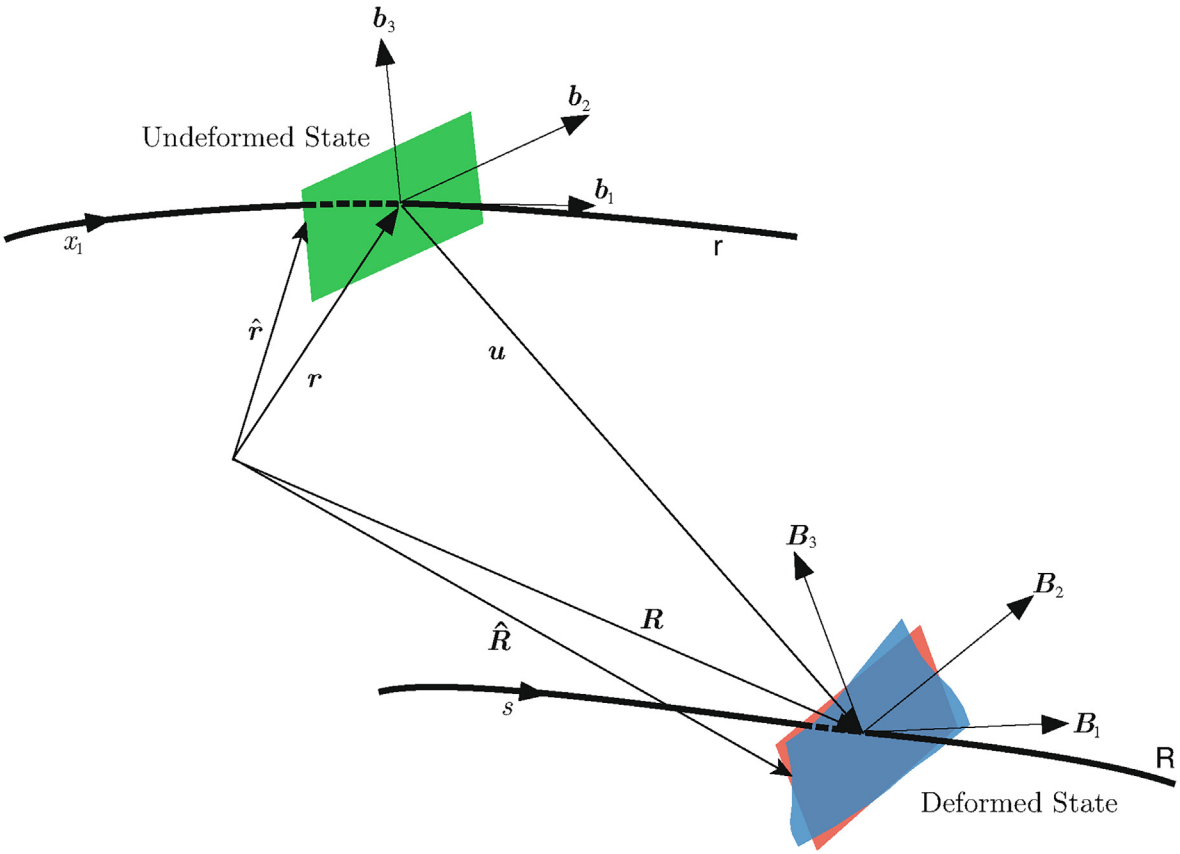

Fig. 2. Sketch of beam kinematics (Hodges, 2003).

We used the aerodynamic model of Peters et al. (1995), which is a state-space, thin-airfoil, inviscid, incompressible approximation of an infinite-state representation of the aerodynamic loads. The model assumes that the airfoil parameters are known, and takes into account the effect of apparent mass and the induced flow in the wake. Additionally, the model accommodates large motions of the wing and small deformation of the airfoil to simulate the aircraft flight control surfaces such as ailerons, flaps, etc. Studies (Sotoudeh et al., 2010; Mardanpour et al., 2013) indicate that this model approximates very well the aerodynamic loads acting on high-aspect-ratio wings. The lift, drag and pitching moment at the quarter-chord of the airfoil are given by

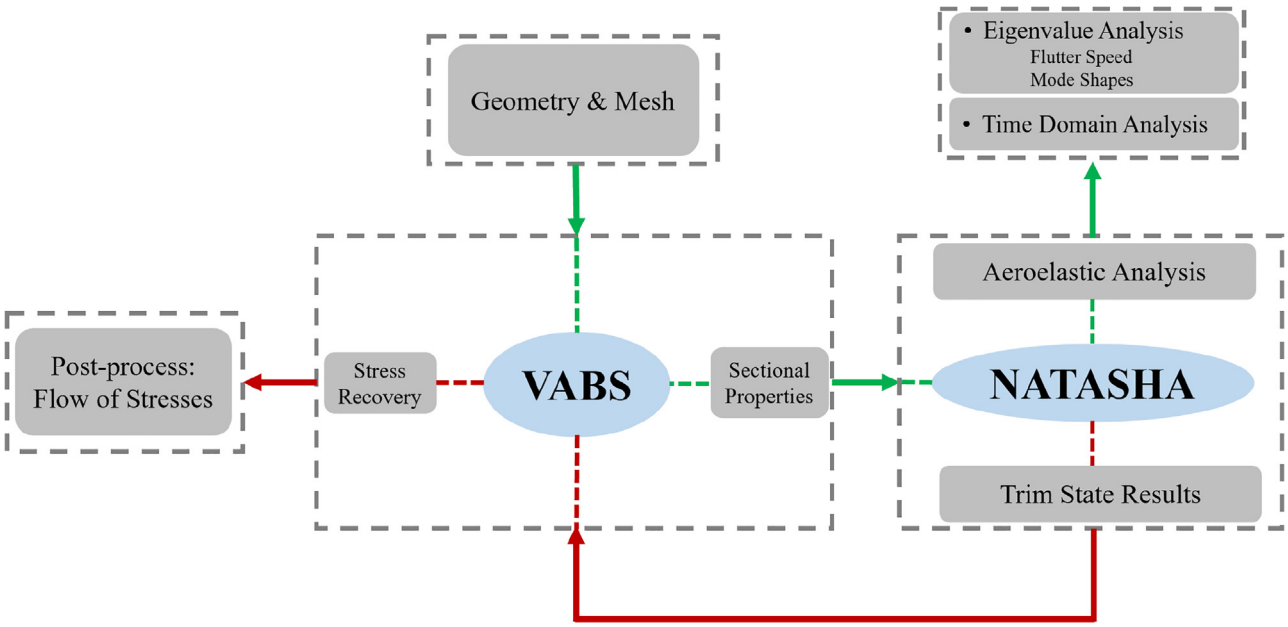

Fig. 3. Overall view of the steps in the numerical procedure.

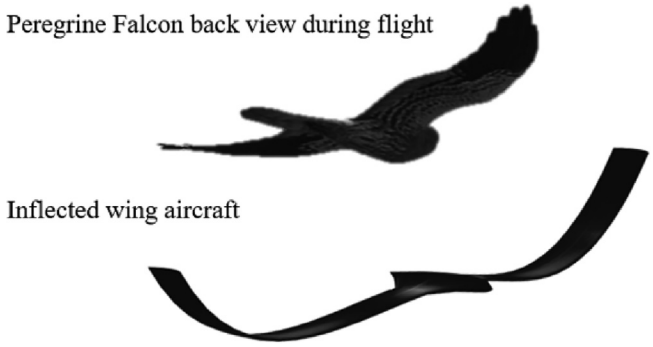

Fig. 4. Peregrine Falcon in cruise flight with inflected wings and designed inflected wing aircraft.

$$L_{\text{aero}} = \rho b\Big[\Big(c_{l_0} + c_{l_\beta}\beta\Big)V_T V_{a_2} - c_{l_\alpha}\dot{V}_{a_3} b/2 - c_{l_\alpha} V_{a_2}\big(V_{a_3} + \lambda_0 - \Omega_{a_1} b/2\big) - c_{d_0} V_T V_{a_3}\Big] \tag{6}$$

$$D_{\text{aero}} = \rho b\Big[-\Big(c_{l_0} + c_{l_\beta}\beta\Big)V_T V_{a_3} + c_{l_\alpha}\big(V_{a_3} + \lambda_0\big)^2 - c_{d_0} V_T V_{a_2}\Big] \tag{7}$$

$$M_{\text{aero}} = 2\rho b\big[(c_{m_0} + c_{m_\beta}\beta)V_T - c_{m_\alpha} V_T V_{a_3} - bc_{l_\alpha}/8 V_{a_2}\Omega_{a_1} - b^2 c_{l_\alpha}\dot{\Omega}_{a_1}/32 + bc_{l_\alpha}\dot{V}_{a_3}/8\big] \tag{8}$$

where

$$V_T = \Big(V_{a_2}^2 + V_{a_3}^2\Big)^{\frac{1}{2}} \tag{9}$$

$$\sin\alpha = \frac{-V_{a_3}}{V_T} \tag{10}$$

$$\alpha_{\text{rot}} = \frac{\Omega_{a_1} b/2}{V_T} \tag{11}$$

and β is the angle of flap deflection, and V_{a_2} and V_{a_3} denote the values of V_a. The effect of the unsteady wake (the induced flow) and the apparent mass appear as λ_0 and acceleration terms in the force and moment equation. The induced flow model (Peters et al., 1995) is used to calculate λ_0:

$$[A_{\text{inducedflow}}]\{\dot{\lambda}\} + \left(\frac{V_T}{b}\right)\{\lambda\} = \left(-\dot{V}_{a_3} + \frac{b}{2}\dot{\Omega}_{a_1}\right)\{c_{\text{inducedflow}}\} \tag{12}$$

$$\lambda_0 = \frac{1}{2}\{b_{\text{inducedflow}}\}^T\{\lambda\} \tag{13}$$

Here λ is the column matrix of induced flow states, and $[A_{\text{inducedflow}}]$, and $\{c_{\text{inducedflow}}\}, \{b_{\text{inducedflow}}\}$ are constant matrices, available in Ref. Peters et al. (1995).

Coupling the aerodynamic equations with the structural equations yields the aeroelastic system:

$$[A]\{\dot{x}\} + \{B(x)\} = \{f_{cont}\} \tag{14}$$

where $\{x\}$ and $\{f_{cont}\}$ are the vectors of the aeroelastic variables and the flight controls, respectively. The resulting nonlinear ordinary differential equations are then linearized about a static equilibrium state, which is obtained by nonlinear algebraic equations.

The stability of the structure is obtained by linearizing this system of nonlinear aeroelastic equations about the resulting equilibrium state, which leads to the standard eigenvalue problem,

$$[A]\{\dot{\hat{x}}\} + [B]\{\hat{x}\} = \{\hat{f}_{cont}\} \tag{15}$$

where $\hat{()}$ is the perturbation about the steady-state values. The steady-state condition is the equilibrium condition, where all the

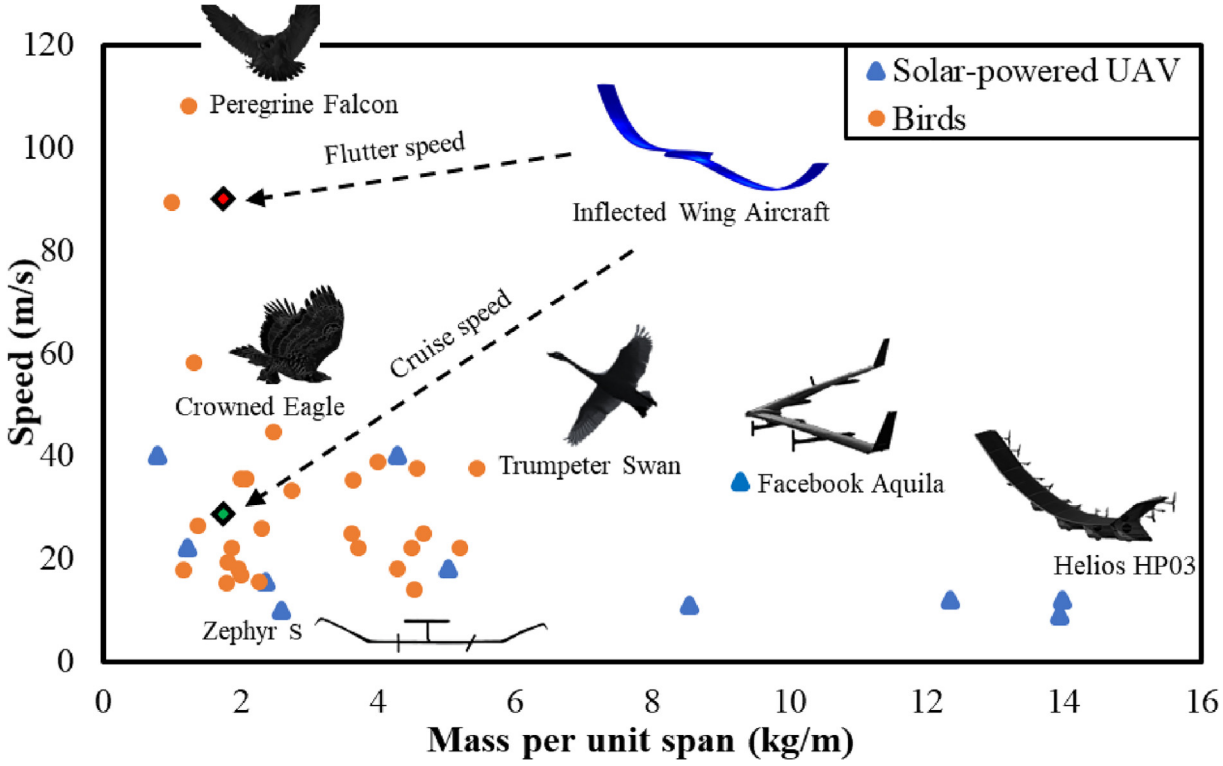

Fig. 5. Mass per unit span versus the flight speed of birds and solar-powered aircraft. Data of birds in-clude subspecies of Goose, Pelican, Eagle, Cormorant, Heron, Albatross, Condor, Swan, and Falcon.

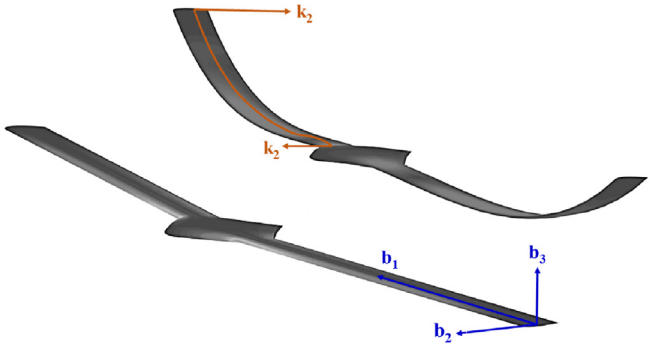

Fig. 6. Flying wing with inflection (top) and without inflection (bottom).

time-derivatives are zero (Patil and Hodges, 2006). The flight dynamic equations of the aircraft are

$$g_2V_2 + g_3V_3 - \tan\phi(g_3V_2 - g_2V_3) = 0 \tag{16}$$

$$V_2^2 + V_3^2 - V_\infty^2 = 0 \tag{17}$$

where ϕ and V_∞ are the prescribed flight angle and airspeed, respectively.

Fig. 3 presents the steps that we followed in the numerical work. The cross-sectional properties of the high-aspect-ratio wing were obtained using VABS (Yu et al., 2002a; Yu and Hodges, 2005; Yu et al., 2012) which is a commercial software designed to compute the sectional properties of slender composite bodies (i.e., a 2D problem), and also obtain an asymptotically exact 3D solution. It does this using the variational method that transforms the 3D slender solid into a 2D cross-sectional analysis. This technique produces results with high accuracy and reduces the computational time significantly.

We used a three-dimensional finite element mesh generator, Gmsh (Geuzaine and Remacle, 2009), to create the geometry and mesh of the cross-section of the fuselage and the wings for each model. With the geometry, mesh and material properties known, VABS calculates the structural and elemental properties. For the corrected cross-sectional properties, we had to input the curvature of each geometry or element into VABS, because the initial twist and curvature of the geometry introduce elastic couplings (Yu et al., 2002b). We then imported the trim state solutions from NATASHA into VABS to obtain the stresses throughout the structure.

4. Inflected wing in nature

High-Altitude Long-Endurance aircraft (HALE) is designed to achieve long-lasting flights at high altitudes. It goes back to the early 1980s (Hall et al., 1983; Youngblood et al., 1982).In order to stay in flight for a long time, some designs benefit from solar energy. Because of the limited energy provided by solar panels distributed over the aircraft, this design should have a very light weight. One of the earliest designs was the Pathfinder solar-powered aircraft. Pathfinder underwent a series of updates and finally the design changed to Helios HP03. In June 2003, the Helios prototype, crashed during the flight test (Noll et al., 2004, 2007). One of the recent designs of this type is the Zephyr aircraft, which has a flight endurance record of more than 25 days.

In Fig. 4, we show the Peregrine Falcon during flight: notice that it has the inflected configuration in its wings, which is very much like the inflected wing aircraft designed in this study. To compare the evolutionary design of solar power aircraft with design in nature, in Fig. 5 we put together the mass per unit span versus the flight speed of birds with the data available for solar-powered UAVs. This figure highlights the ability of Peregrine Falcon to fly at high speeds, while it has a very small mass per unit span ratio. Furthermore, the figure illustrates the very large mass per unit span ratio of Helios HP03, which crashed in 2003. Zephyr aircraft, which holds the record of flight endurance, has a small mass per unit span ratio, but its main disadvantage is very low speed. The

Table 2
Inflection values (rad/m) for different test cases.

Case Number	Curvature at Root	Curvature at Tip
1	0	0
2	0.02	−0.04
3	0.03	−0.06
4	0.07	−0.18
5	0.05	−0.14
6	0.05	−0.15
7	0.1	−0.2

Table 1
Properties of the wing configuration without inflection.

	Wing	Fuselage
Span [m]	16	4
Chord [m]	1	4
Sweep Angle	5°	–
ξ [m]	$\begin{bmatrix} 0 \\ 1.13\times10^{-01} \\ 1.25\times10^{-17} \end{bmatrix}$	$\begin{bmatrix} 0 \\ 2.83\times10^{-01} \\ -8.02\times10^{-18} \end{bmatrix}$
I [kg.m]	$\begin{bmatrix} 1.56\times10^{-01} & 0 & 0 \\ 0 & 2.34\times10^{-03} & -1.69\times10^{-18} \\ 0 & -1.69\times10^{-18} & 1.54\times10^{-01} \end{bmatrix}$	$\begin{bmatrix} 8.53 & 0 & 0 \\ 0 & 1.13\times10^{-01} & -1.44\times10^{-16} \\ 0 & -1.44\times10^{-16} & 8.42 \end{bmatrix}$
T [N^{-1}-m^{-2}]	$\begin{bmatrix} 3.48\times10^{-06} & 0 & 0 \\ 0 & 4.27\times10^{-06} & -6.66\times10^{-14} \\ 0 & -6.66\times10^{-14} & 6.51\times10^{-08} \end{bmatrix}$	$\begin{bmatrix} 1.30\times10^{-07} & 0 & 0 \\ 0 & 1.60\times10^{-07} & -2.49\times10^{-15} \\ 0 & -2.49\times10^{-15} & 2.44\times10^{-09} \end{bmatrix}$
R [N^{-1}]	$\begin{bmatrix} 7.24\times10^{-09} & 0 & 0 \\ 0 & 2.58\times10^{-08} & 1.76\times10^{-13} \\ 0 & 1.75\times10^{-13} & 9.66\times10^{-07} \end{bmatrix}$	$\begin{bmatrix} 1.31\times10^{-09} & 0 & 0 \\ 0 & 4.66\times10^{-09} & 3.17\times10^{-14} \\ 0 & 3.17\times10^{-14} & 1.74\times10^{-07} \end{bmatrix}$
S [N^{-1}-m^{-1}]	$\begin{bmatrix} 0 & -7.55\times10^{-15} & 7.37\times10^{-09} \\ -3.34\times10^{-14} & 0 & 0 \\ -1.16\times10^{-06} & 0 & 0 \end{bmatrix}$	$\begin{bmatrix} 0 & -6.11\times10^{-16} & 5.97\times10^{-10} \\ -2.71\times10^{-15} & 0 & 0 \\ -9.41\times10^{-08} & 0 & 0 \end{bmatrix}$

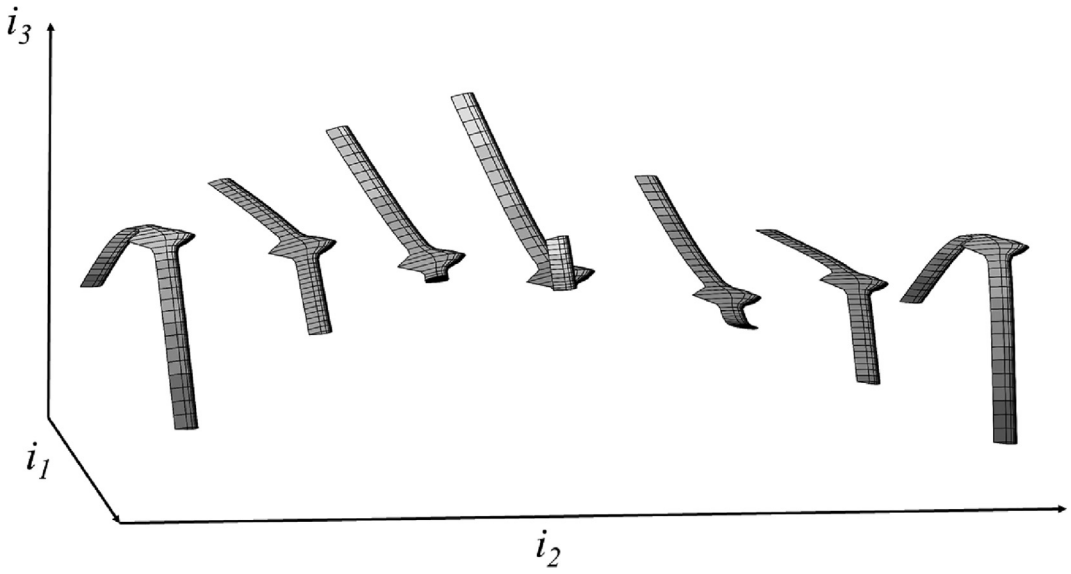

Fig. 7. The body-freedom flutter mode shape of the flying wing aircraft.

Table 3
Flutter speed for different cases.

Case Number	Flutter Speed (m/s)
1	37.3
2	41.1
3	46.4
4	68.2
5	78.9
6	86.2
7	91.7

Table 4
Values of thrust at equilibrium condition (cruise speed 35 m/s).

Case Number	Thrust
1	11.07045547
2	11.07179964
3	11.0738817
4	11.09470655
5	11.08091847
6	11.08228087
7	11.111

mass per unit span versus the flight speed of the inflected configuration (designed in this study) reveals a promising change in the evolutionary design of highly-flexible and light-weight aircraft.

5. Case study

We compared the flow of stresses and the aeroelastic stability of a flying wing without inflection with wings that have inflection. Fig. 6 presents 3D views of the models without inflection and with inflection. The wing inflection is the component of curvature vector about $\mathbf{b}_2$. Table 1 lists the properties of the wings and the fuselage elements of the flying wing configuration without inflection. Since the fuselage is a tapered geometry, we presented the properties of the elements at the center of the fuselage. One can examine the properties of other elements by interpolation between the values at the center of the fuselage and the wings. The wingspan, chord, and sweep angle are the same for all configurations (inflected and not inflected).

Table 2 shows the inflection (the flap-wise component of the curvature vector) introduced in six test cases. These values are the components of the curvature vector in the $\mathbf{b}_2$ direction at the root and the tip of the wing, and they vary linearly along the wing.

6. Results and discussion

This section presents the results of the flutter and stress analyses for the flying wing without inflection and the six other configurations with inflection. We found that the base model with no inflection flutters at 37.3 m/s with a frequency of 4.7 rad/s.

The aircraft exhibited dynamic instabilities that involve the elastic modes of the wing coupled with the rigid body motion of the aircraft, which has been called “body-freedom flutter” shown in Fig. 7.

Table 3 shows the flutter speed of the base model aircraft (i.e., wing without inflection) and the flying wing configurations with different wing inflections. The chief conclusion is that the wing with no inflection has the lowest flutter speed while the inflected wing configurations have higher flutter speed.

The simulation software NATASHA determined the equilibrium condition of the models at 35 m/s and assessed the stability of the system. NATASHA finds the equilibrium configuration for the equality of drag to thrust and weight to lift. At this speed, the values of required thrust are presented in Table 4. The changes in required thrust (drag) due to the addition of inflection are negligible.

For the flying wing aircraft to stay in the equilibrium state, NATASHA computes the values of flap deflection and angle of attack to compensate for losses in the lift. Fig. 8 shows that for most cases the angle of attack decreases as we add inflection. Additionally, Fig. 9 presents the necessary flap deflection angle for each case. The maximum flap deflection angle is 5 degrees, which is required in case 6. These figures indicate that there is not a linear relation between inflection and lift and drag.

After the results of the equilibrium condition, the computer program VABS calculates the stresses distribution. We plotted the most relevant stress distributions in Figs. 10–13.

Fig. 10 shows the stress distribution for σ_{11} for the complete flying body. The case without curvature is experiencing a high concentration of stresses at the roots of the wings. The addition of inflection to the structure changes completely the flow pattern of

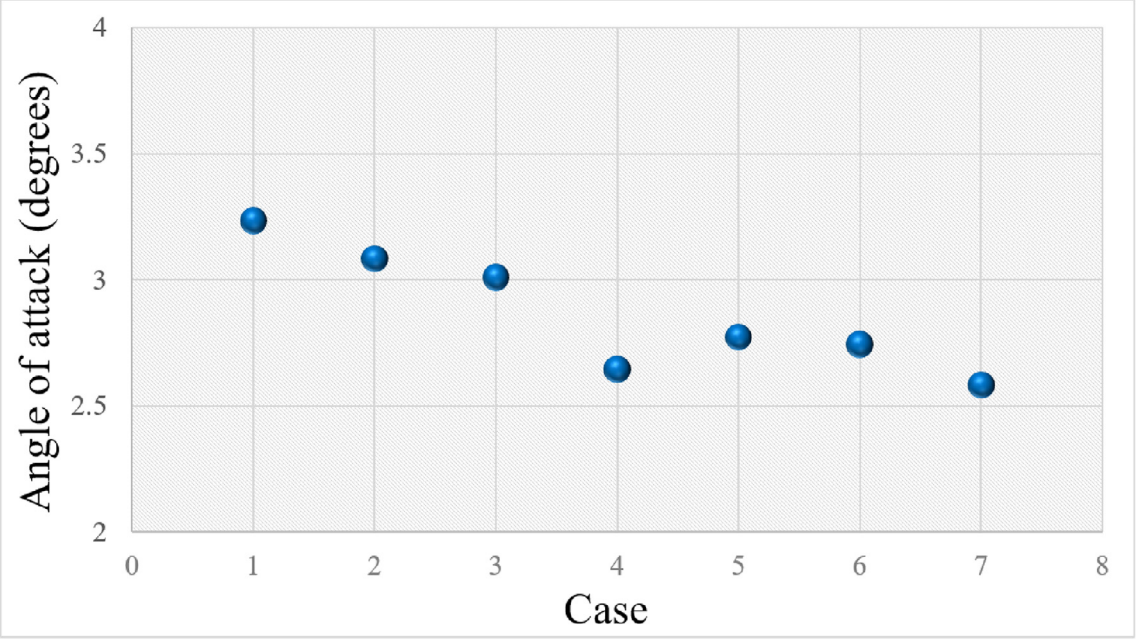

Fig. 8. Values of angle of attack at equilibrium condition (cruise speed 35 m/s).

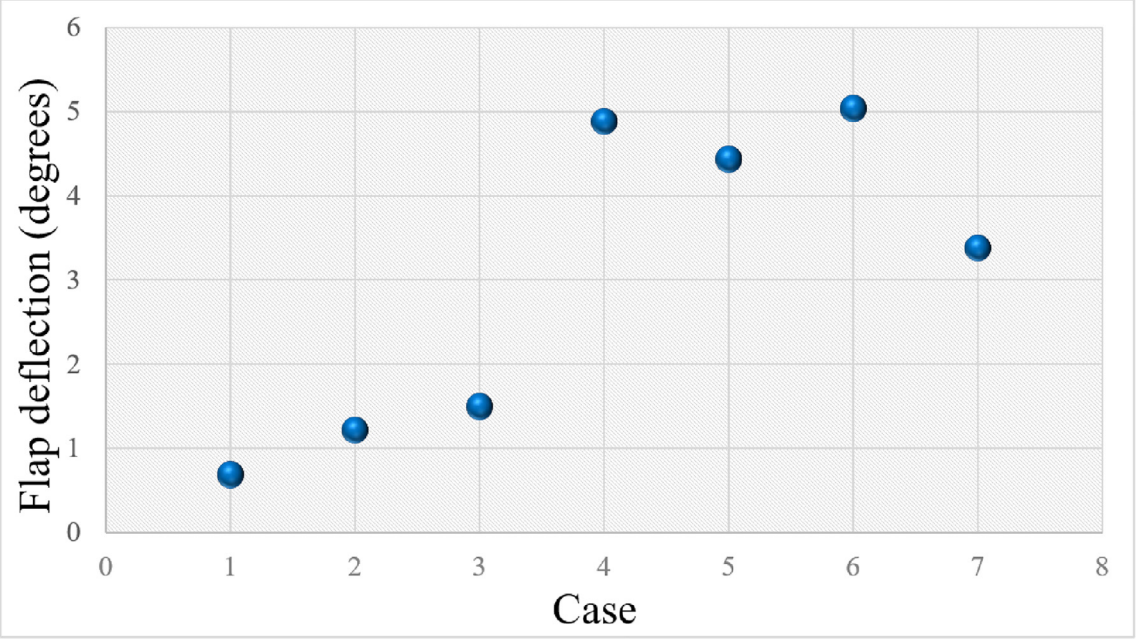

Fig. 9. Values of flap deflection at equilibrium condition (cruise speed 35 m/s).

the stresses σ_{11}. The concentration at the root begins to smooth out in configurations with inflection(cases 2–7). By increasing the inflection, the strangulation at the root begins to disappear and the concentration of stresses moves to the mid-span of the wing. Although the concentration of stress at the mid-span persists, the magnitude of the stress is significantly smaller than in cases 1, 2 and even 3.

Fig. 11 shows the distribution of stresses σ_{12} for the complete flying body. For the σ_{12} component of the stress tensor the strangulation still occurs. Cases 4 and 7 have the larger inflection values and also the greater stress strangulation in the wings. However, in all cases, σ_{12} is one order of magnitude smaller than σ_{11}.

In Fig. 12 we see the distribution of the stresses σ_{13}, which is two orders of magnitude smaller than the stresses σ_{11}. There is not a significant difference between the stress distribution of cases 1 through 6; only case 7 exhibits the highest stress concentration and, consequently, has the least uniform stress distributions.

Finally, in Fig. 13 we see the distribution of the Von Mises stresses that are of the same order of magnitude as the stresses σ_{11}. Case 1 reveals the presence of stress strangulation with large magnitudes at the root of the wings. The strangulation at the roots starts to smooth out for cases 2 and 3, while there is no strangulation of Von Mises stress for cases 4 to 7. It is worth noting that cases 2 and 3 have the smallest inflection.

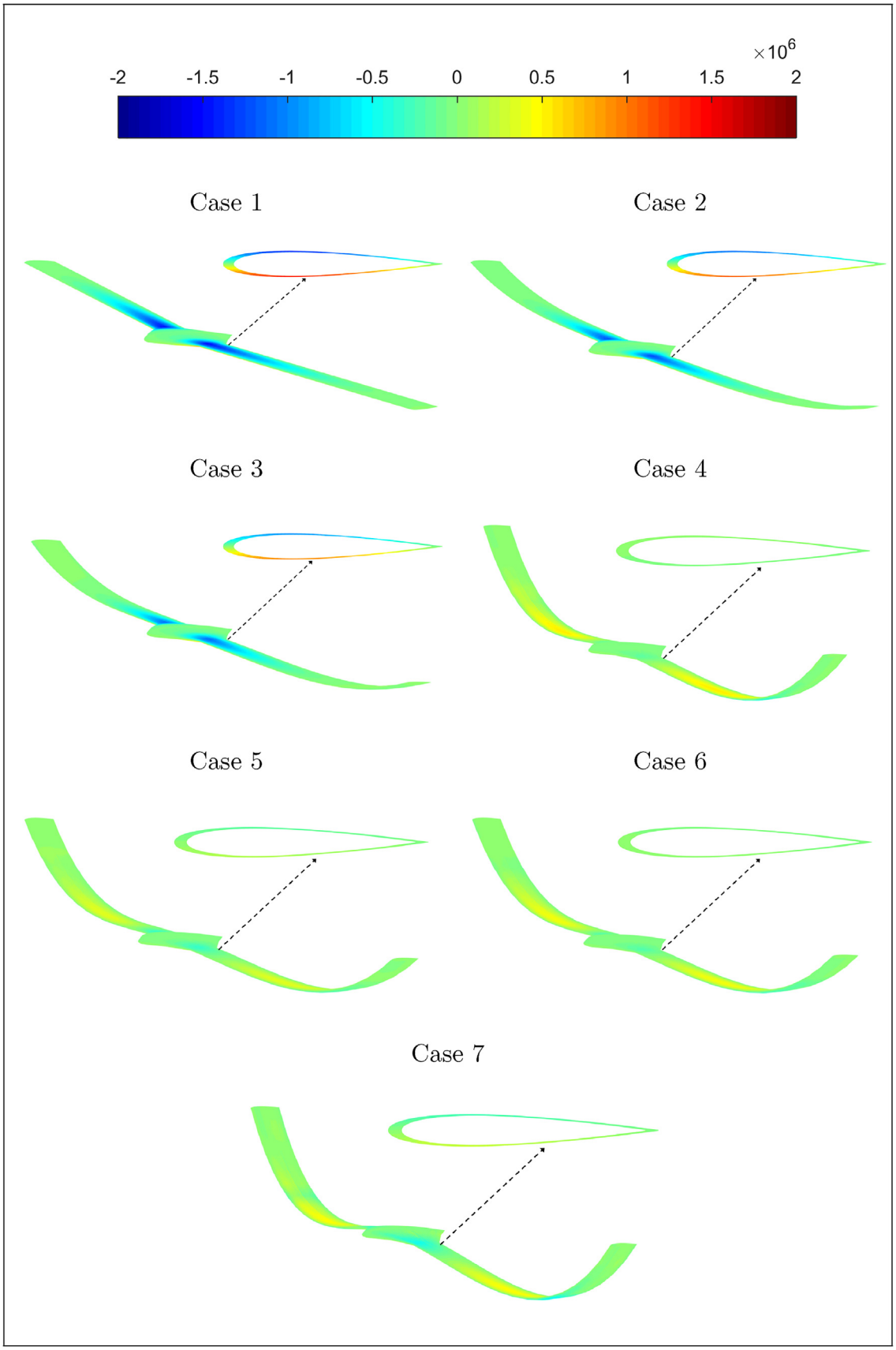

Fig. 10. Distribution of stresses σ_{11} (Pa) in the flying wing.

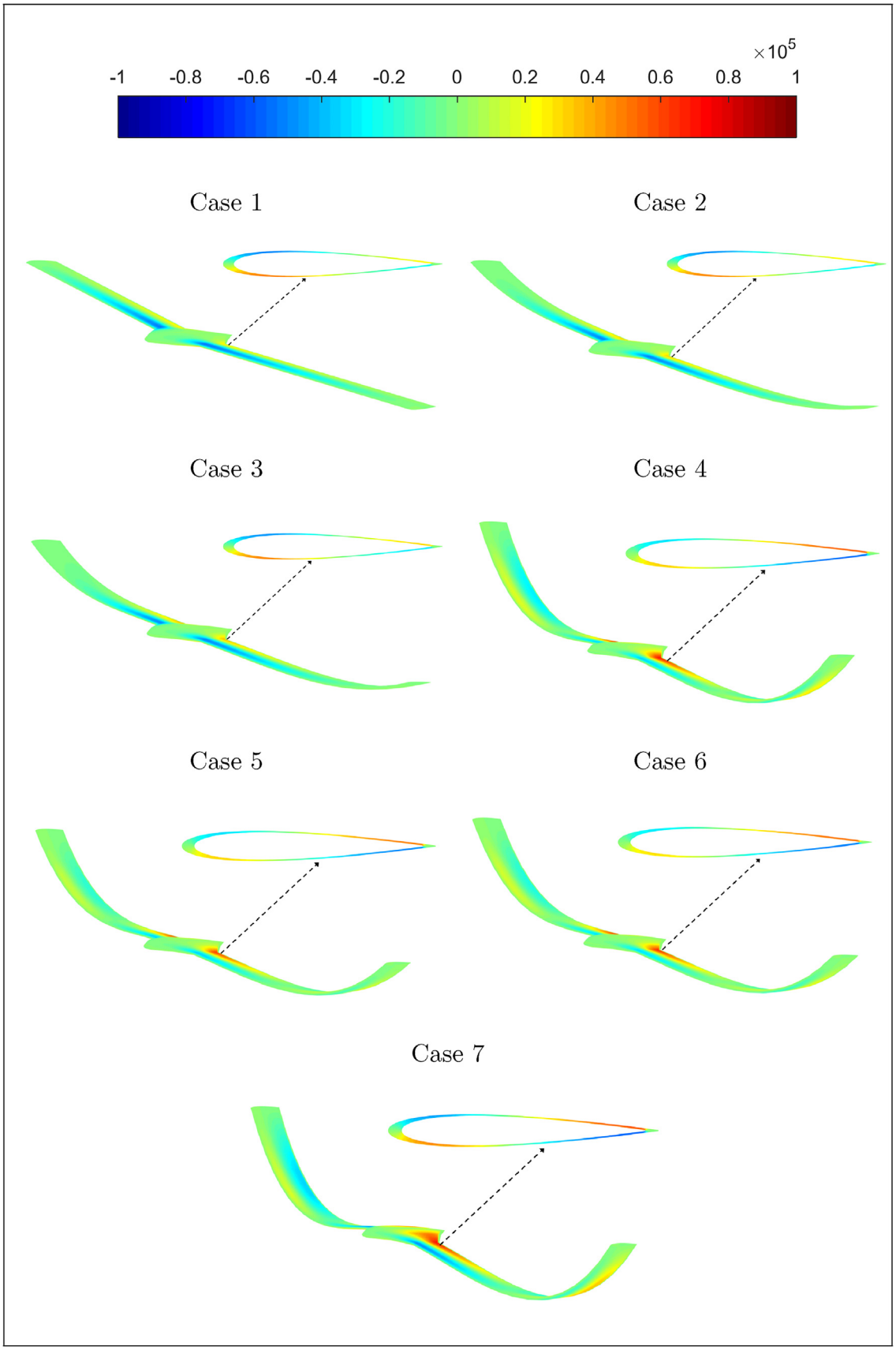

Fig. 11. Distribution of stresses σ_{12} (Pa) in the flying wing.

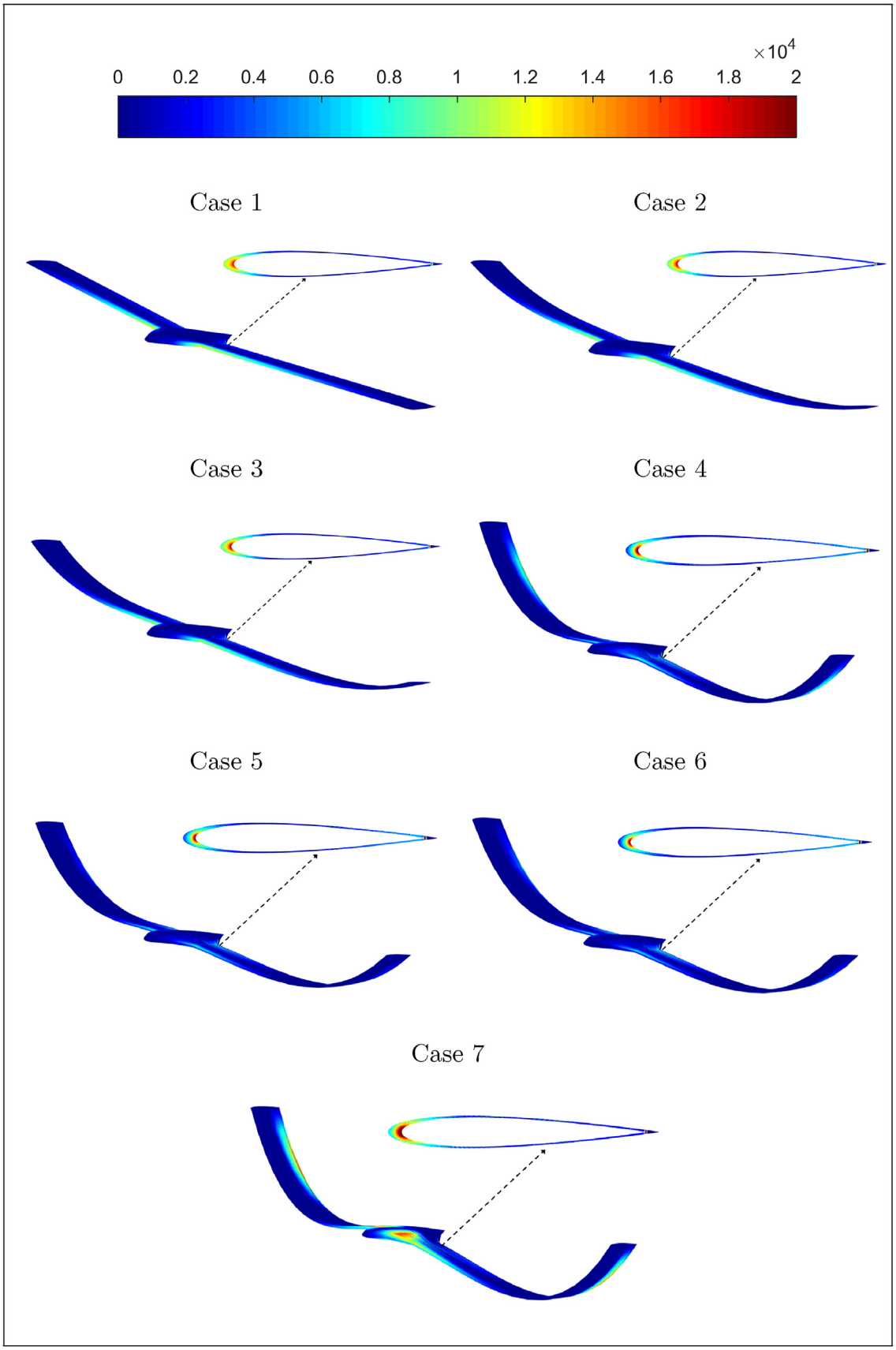

Fig. 12. Distribution of stresses σ_{13} (Pa) in the flying wing.

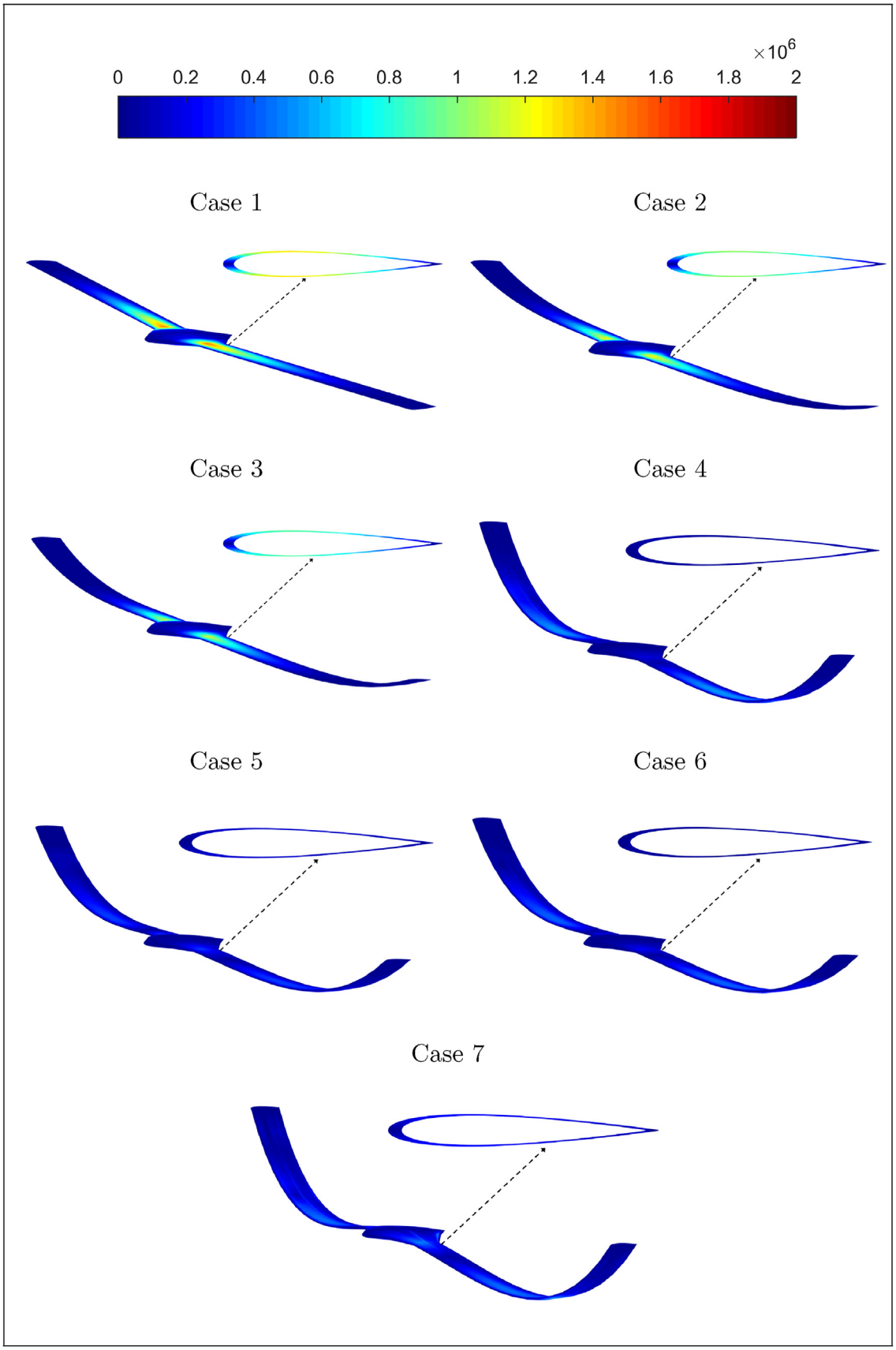

Fig. 13. Distribution of Von Mises stresses (Pa) in the flying wing.

7. Conclusion

In this study we unveiled the relationship between the freedom to morph the wing in flight and the stability (flutter speed) of the wing. We showed that inflected wings have the potential to enhance significantly the stability of the flying body.

In addition, avoidance of flutter is a relevant consideration for understanding the design of the wings of flying animals, for several reasons:

First is noiseless flight, as in the cases studied by Jaworski and Peake (Jaworski and Peake, 2013, 2020). These extensive studies refer to owls and like predators, however, the design of noiseless approach is generally relevant in predator design, terrestrial and aquatic as well. In all these cases, stealth in sound is achieved the way the owl achieves it: by morphing its wing and feathers to go with the structure of the large scale turbulence generated in their immediate vicinity.

The additional payback from understanding this goes to developers of future human flight, not by copying birds, but by implementing the design principle on which the bird wing is constructed. That principle is this: more freedom to morph to go with the turbulent flow (much more freedom than the developers of aircraft contemplate of implementing in their designs).

Our contribution is that the avoidance of flutter (through morphing the wings) is the result of distributing all the stresses more uniformly throughout the wing and the rest of the flying body. The bigger payoff from uniform stresses (in addition to avoiding flutter) is reduced weight. The flying animal like the aircraft, is considerably more economical when svelte, with minimal but necessary structural weight to carry. Of course, animal design has evolved admirably in this direction of survivability during its big history, yet the secret for its success (uniform stress distribution, and freedom to morph in all space and time) does not become evident unless we demonstrate it, one feature at a time, as in our present study.

We are discovering that by making the above observation we arrive at the symbiosis of biology and engineering science. Our hope is that studies such as the present one will make the symbiosis better known and more useful in both domains. This great quote captures the truth: “Where an engineer sees design, a biologist sees natural selection” (John Maynard Smith).

Finally, there are differences in scale and speed between flying wings, animal and aircraft, small and big in each domain. The usefulness of the present work has a lot to do with the fact that today the scaling-up and scaling-down rules of locomotion (air, land, water) are well known, and they are reliable.

Many cases of inflected wings aircraft were tested, and the most relevant ones were presented. Noteworthy is that a “predictive design theory” is required to see that inflection values increase the flutter speed. This research sheds light on importance of inflection which could lead to future technology development.

The physical basis for the difference between the two flying configurations (inflected vs. not inflected) is that (because of the freedom to morph in space and time) the inflected wing has a considerably more uniform distribution of stresses through its body. This endows the inflected wing with additional advantageous such as svelteness, light weight and strength.

In sum, the study illustrates the close relationship between animal design and vehicle design. The evolution of aircraft design has been influenced from the start by the design of animal flight. Presently, inflected wings belong in the animal realm, not in machine flight. In the present study we relied on the theory of aeroelasticity and computational techniques developed in physics and engineering. The results are relevant to and applicable in two domains, aircraft design and animal design. In this way, aircraft design returns the favor to its original source of inspiration, and sheds light on the physics that underpins the unmatched performance of animal design.

CRediT authorship contribution statement

Pezhman Mardanpour: Conceptualization, Data curation, Formal analysis, Funding acquisition, Methodology, Project administration, Software, Supervision, Validation, Visualization, Writing - original draft, Writing - review & editing. **Ehsan Izadpanahi:** Data curation, Formal analysis, Investigation, Visualization, Writing - original draft. **Shanae Powell:** Formal analysis, Investigation, Visualization, Writing - original draft. **Siavash Rastkar:** Writing - original draft. **Adrian Bejan:** Conceptualization, Visualization, Writing - original draft, Writing - review & editing.

Acknowledgment

Professor Mardanpour’s research is supported by the U.S. Air Force Office of Scientific Research and the U.S. National Science Foundation.

References

Agrawal B.R., Sharma A., 2016. Numerical investigations of bio-inspired blade designs to reduce broadband noise in aircraft engines and wind turbines. In: 54th AIAA Aerospace Sciences Meeting, p. 0760..
Ahlborn, B., 2004. Zoological Physics. Springer, Berlin.
Bejan, A., 2016. The Physics of Life: The Evolution of Everything. St. Martins Press, New York City.
Bejan, A., 2020. Freedom and Evolution. Springer Nature, Switzerland.
Bejan, A., Lorente, S., 2008. Design with Constructal Theory. Wiley, Hoboken.
Bejan, A., Marden, J.H., 2006. Unifying constructal theory for scale effects in running, swimming and flying. Journal of Experimental Biology 209, 238–248.
Bejan, A., Marden, J.H., 2009. The constructal unification of biological and geophysical design. Physics of Life Reviews 6, 85–102.
Bejan, A., Lorente, S., Lee, J., 2008. Unifying constructal theory of tree roots, canopies and forests. Journal of Theoretical Biology 254, 529–540.
Chang, C.-S., Hodges, D.H., Patil, M.J., 2008. Flight dynamics of highly flexible aircraft. Journal of Aircraft 45, 538–545.
Chiarelli M.R., Cagnoni M., Ciabattari M., De Biasio M., Massai A., 2009. Preliminary analysis of a high aspect ratio wing with curved planform. In: AIDAA, Milan, Italy..
Chiarelli M., Lombardi G., Nibio A., 2011. A straight wing and a forward swept wing compared with a curved planform wing in the transonic regime. In: CEAS, Venice, Italy..
Chin, D.D., Lentink, D., 2016. Flapping wing aerodynamics: from insects to vertebrates. Journal of Experimental Biology 219, 920–932.
Dora, M., 2018. An investigation on naca 2312 aerofoil with curved and straight leading edge wing. International Journal of Research 5, 2435–2440.
Dudley, R., 2002. The Biomechanics of Insect Flight: Form, Function, Evolution. Princeton University Press.
Hall D.W., Fortenbach C.D., Dimiceli E.V., Parks R.W., 1983. A preliminary study of solar powdered aircraft and associated power trains..
Galantai, V., Sofla, A., Meguid, S., Tan, K., Yeo, W., 2012. Bio-inspired wing morphing for unmanned aerial vehicles using intelligent materials. International Journal of Mechanics and Materials in Design 8, 71–79.
Geuzaine, C., Remacle, J.-F., 2009. Gmsh: A 3-d finite element mesh generator with built-in pre-and post-processing facilities. International Journal for Numerical Methods in Engineering 79, 1309–1331.
Hodges, D.H., 2003. Geometrically exact, intrinsic theory for dynamics of curved and twisted anisotropic beams. AIAA Journal 41, 1131–1137.
Izadpanahi, E., Mardanpour, P., 2018. Nonlinear aeroelastic response of highly flexible flying wing due to different gust loads. In: Reyhanoglu, M. (Ed.), Nonlinear Systems. IntechOpen, pp. 89–106.
Jaworski, J.W., Peake, N., 2013. Aerodynamic noise from a poroelastic edge with implications for the silent flight of owls. Journal of Fluid Mechanics 723, 456–479.
Jaworski, J.W., Peake, N., 2020. Aeroacoustics of silent owl flight. Annual Review of Fluid Mechanics 52, 395–420.
Kasimova, R., Tishin, D., Obnosov, Y.V., Dlussky, G., Baksht, F., Kacimov, A., 2014. Ant mound as an optimal shape in constructal design: Solar irradiation and circadian brood/fungi-warming sorties. Journal of Theoretical Biology 355, 21–32.
Khan, M.M.I., Al-Faruk, A., 2018. Comparative analysis of aerodynamic characteristics of rectangular and curved leading edge wing planforms. American Journal of Engineering Research 7, 281–291.

Lentink, D., Müller, U., Stamhuis, E., De Kat, R., Van Gestel, W., Veldhuis, L., Henningsson, P., Hedenström, A., Videler, J.J., Van Leeuwen, J.L., 2007. How swifts control their glide performance with morphing wings. Nature 446, 1082.

Lilley G.M., 1998. A study of the silent flight of the owl, AIAA paper 2340 l–6..

Lorente, S., Lee, J., Bejan, A., 2010. The "flow of stresses" concept: the analogy between mechanical strength and heat convection. International Journal of Heat and Mass Transfer 53, 2963–2968.

Mandadzhiev, B.A., Lynch, M.K., Chamorro, L.P., Wissa, A.A., 2017. An experimental study of an airfoil with a bio-inspired leading edge device at high angles of attack. Smart Materials and Structures 26. 094008.

Mardanpour, P., Hodges, D.H., Neuhart, R., Graybeal, N., 2013. Engine placement effect on nonlinear trim and stability of flying wing aircraft. Journal of Aircraft 50, 1716–1725.

Mardanpour, P., Richards, P.W., Nabipour, O., Hodges, D.H., 2014. Effect of multiple engine placement on aeroelastic trim and stability of flying wing aircraft. Journal of Fluids and Structures 44, 67–86.

Mardanpour, P., Izadpanahi, E., Rastkar, S., Hodges, D.H., 2017a. Effects of engine placement on nonlinear aeroelastic gust response of high-aspect-ratio wings. In: AIAA Modeling and Simulation Technologies Conference. Texas, Grapevine, p. 0576.

Mardanpour, P., Izadpanahi, E., Rastkar, S., Hodges, D.H., 2017b. Nonlinear aeroelastic gust suppression and engine placement. Journal of Aircraft 54, 2402–2404.

Mardanpour, P., Izadpanahi, E., Rastkar, S., Calastawad, S., Levy, C., 2018. Effect of shooting and blast-induced gust on nonlinear aeroelastic stability and behavior of high-aspect ratio wing. Journal of Sound and Vibration 433, 299–313.

Chiarelli M.R., Cagnoni M., Ciabattari M., De Biasio M., Massai A., 2010. High aspect ratio wing with curved planform: Cfd and fe analyses. In: ICAS, Nice, France..

Miguel, A.F., 2006. Constructal pattern formation in stony corals, bacterial colonies and plant roots under different hydrodynamics conditions. Journal of Theoretical Biology 242, 954–961.

Miguel, A.F., 2016. Toward an optimal design principle in symmetric and asymmetric tree flow networks. Journal of Theoretical Biology 389, 101–109.

Nguyen, N., Trinh, K., Reynolds, K., Kless, J., Aftosmis, M., Urnes, J., 2013. Elastically shaped wing optimization and aircraft concept for improved cruise efficiency. In: 51st AIAA Aerospace Sciences Meeting Including the New Horizons Forum and Aerospace Exposition, p. 141.

Noll, T.E., Brown, J.M., Perez-Davis, M.E., Ishmael, S.D., Tiffany, G.C., Gaier, M., 2004. Investigation of the helios prototype aircraft mishap volume i mishap report 9.

Noll T.E., Ishmael S.D., Henwood B., Perez-Davis M.E., Tiffany G.C., Madura J., Gaier M., Brown J.M., Wierzbanowski T., 2007. Technical findings, lessons learned, and recommendations resulting from the helios prototype vehicle mishap, Technical Report, National Aeronautics and Space Admin Langley Research Center Hampton VA..

Patil, M.J., Hodges, D.H., 2006. Flight dynamics of highly flexible flying wings. Journal of Aircraft 43, 1790–1799.

Peters, D.A., Karunamoorthy, S., Cao, W.-M., 1995. Finite state induced flow models. i-two-dimensional thin airfoil. Journal of Aircraft 32, 313–322.

Reis, A.H., Miguel, A.F., Aydin, M., 2004. Constructal theory of flow architecture of the lungs. Medical Physics 31, 1135–1140.

Schmidt-Nielsen, K., 1984. Scaling: Why is Animal Size So Important? Cambridge University Press, Cambridge, UK.

Sofla, A., Meguid, S., Tan, K., Yeo, W., 2010. Shape morphing of aircraft wing: Status and challenges. Materials & Design 31, 1284–1292.

Sotoudeh, Z., Hodges, D.H., Chang, C.-S., 2010. Validation studies for aeroelastic trim and stability of highly flexible aircraft. Journal of Aircraft 47, 1240–1247.

Van Dam, C., 1987. Induced-drag characteristics of crescent-moon-shaped wings. Journal of Aircraft 24, 115–119.

Vogel, S., 1988. Life's Devices: The Physical World of Animals and Plants. Princeton University Press, Princeton, NJ.

Wainwright, S.A., Biggs, W.D., Currey, J.D., Gosline, J.M., 1976. Mechanical Design in Organisms. Edward Arnold, London.

Weibel, E.R., Taylor, C.R., Bolis, L., 1998. Principles of Animal Design. Cambridge University Press, Cambridge, UK.

Youngblood J., Talay T., 1982. Solar-powered airplane design for long-endurance, high-altitude flight. In: 2nd International Very Large Vehicles Conference, p. 811..

Yu, W., Hodges, D.H., 2005. Generalized timoshenko theory of the variational asymptotic beam sectional analysis. Journal of the American Helicopter Society 50, 46–55.

Yu, W., Volovoi, V.V., Hodges, D.H., Hong, X., 2002a. Validation of the variational asymptotic beam sectional analysis. AIAA Journal 40, 2105–2112.

Yu, W., Hodges, D.H., Volovoi, V., Cesnik, C.E., 2002b. On timoshenko-like modeling of initially curved and twisted composite beams. International Journal of Solids and Structures 39, 5101–5121.

Yu, W., Hodges, D.H., Ho, J.C., 2012. Variational asymptotic beam sectional analysis–an updated version. International Journal of Engineering Science 59, 40–64.